Chapter 2

Heavy Quarkonium Spectroscopy

2.1 Introduction

Quarkonia are the flavorless mesons that have both quark and antiquark of the same type making them the best tools for understanding the dynamics of strongly interacting systems. The first quarkonium state J/ψ ($c\bar{c}$ or charmonia) was discovered experimentally and announced by Stanford Linear Accelerator Center and Brookhaven National Laboratory on November 11, 1974 [61]. The E760 collaboration at Fermilab measured the masses as well as the total widths of P states namely χ_{c1} and χ_{c2} [62]. Then, the 1^3D_2 state was discovered in B decays by BESIII collaboration [63]. The first ground state singlet charmonium η_c was also discovered in Mark-II and Crystal ball experiments. Similarly, Υ ($b\bar{b}$ or bottomonia) was first discovered by E288 at Fermilab [64, 65]. After 30 years, the first singlet state $\eta_b(1S)$ was discovered by Belle Collaboration [66] in 2008. Later, $\eta_b(2S)$ was also discovered by *BABAR* [67], CLEO [68] and Belle [69] collaborations. Also in 90's, the nonrelativistic potential models predicted not only the ground state mass of the tightly bound state of c and $\bar{b}$ in the range of 6.2–6.3 GeV [70, 71], but also predicted to have very rich spectroscopy. In 1998, CDF collaboration [72] reported B_c mesons in $p\bar{p}$ collisions at $\sqrt{s} = 1.8$ TeV and was later confirmed by D0 [73] and LHCb [74] collaborations. The LHCb collaboration has also made the most precise measurement of the lifetime of B_c mesons [75]. Its first excited state has also been reported by ATLAS Collaborations [76] in $p\bar{p}$ collisions with significance of 5.2σ. Many experimental groups such as CLEO, LEP, CDF, D0 and NA50 have provided data and *BABAR*, Belle, CLEO-III, ATLAS, CMS and LHCb are producing and expected to produce more precise data in upcoming experiments, particularly for the heavy

quarkonium physics. Comprehensive reviews on the status of experimental heavy quarkonium physics are found in literature [15, 16, 77–80].

There are many theoretical groups working on the heavy quarkonium spectroscopy as well as its decay properties. The models based on first principles and fully non-perturbative ones such as lattice quantum chromodynamics (LQCD) [2–12], QCD sum rules [45,81] with QCD [82,83], perturbative QCD [84], lattice NRQCD [85,86] and effective field theories [87] that have attempted to explain the production and decays of these states. The other approaches include phenomenological potential models such as the relativistic quark model based on quasi-potential approach [88–94], where the relativistic quasi-potential including one loop radiative corrections reproduce the mass spectrum of quarkonium states. The quasi-potential has also been employed along with leading order radiative correction to heavy quark potential [95–98], relativistic potential model [99–101] as well as semirelativistic potential model [102]. In nonrelativistic potential models, there exist several forms of quark antiquark potentials in the literature. Common element among them is the coulomb repulsive plus quark confinement interaction potential. The authors of [46–50, 103, 104] have considered the confinement of power potential Ar^{ν} with ν varying from 0.1 to 2.0 and the confinement strength A to vary with potential index ν. Confinement of the order $r^{2/3}$ have also been attempted [105]. Linear confinement of quarks has been considered by many groups [35, 37, 106–116] and they have been in good agreement with the experimental data for quarkonium spectroscopy along with decay properties. The Bethe-Salpeter approach was also employed for the mass spectroscopy of charmonia and bottomonia [110, 111, 117]. The quarkonium mass spectrum was also computed in the nonrelativistic quark model [118], screened potential model (SPM) [115,116] and constituent quark model [119]. There are also other non-linear potential models that predict the mass spectra of the heavy quarkonia successfully [36, 43, 44, 120–127].

The interaction potential for mesonic states is difficult to derive for full range of quark antiquark separation from first principles of QCD. So most forms of QCD inspired potential would result in uncertainties in the computation of spectroscopic properties particularly in the intermediate range. Different potential models may produce similar mass spectra matching with experimental observations but they may not be in mutual agreement when it comes to decay properties like decay constants, leptonic decays or radiative transitions. Moreover, the mesonic states are

identified with masses along with certain decay channels, therefore the test for any successful theoretical model is to reproduce the mass spectrum along with decay properties. Relativistic as well as nonrelativistic potential models have successfully predicted the spectroscopy but they are found to differ in computation of the decay properties [35, 36, 43–50].

In this chapter, we employ nonrelativistic potential with one gluon exchange (essentially Coulomb like) plus linear confinement (Cornell potential) as this form of the potential is also supported by LQCD [128–130]. We solve the Schrödinger equation numerically for the potential to get the spectroscopy of the quarkonia. We first compute the mass spectra of charmonia and bottomonia states to determine quark masses and confinement strengths after fitting the spin-averaged ground state masses with experimental data of respective mesons. Using the potential parameters and numerical wave functions, we compute the decay properties such as leptonic decay constants, digamma, dilepton, digluon decay width using the Van-Royen Weiskopf formula. These parameters are then used to compute the mass spectra and lifetime of B_c meson. We also compute the electromagnetic ($E1$ and $M1$) transition widths of heavy quarkonia and B_c mesons. This work was published in European Physical Journal C [131]. We have also computed the decay properties of charmonia and bottomonia in the extended harmonic confinement model (ERHM) [38, 39] as well as in nonrelativistic treatment for Coulomb plus power potential ($CPP_{\nu=1}$) using variational trial wave function [46–49, 132, 133]. This work was also published in Chinese Physics C [134].

2.2 Methodology

The bound state of two body systems in QCD is nonperturbative in nature and only LQCD can explain its properties. However, other methods are also found to exist in literature. The mesonic bound state within relativistic quantum field is described in Bethe-Salpeter formalism but the Bethe-Salpeter equation is solved only in the ladder approximations. Also, Bethe-Salpeter approach in harmonic confinement is successful in low flavor sectors [135, 136]. The alternative, old and still effective approach is the nonrelativistic potential model approach. Sufficiently small momenta of the charm and bottom quark compared to bound state mass of charmonia and bottomonia constitutes the basis of nonrelativistic treatment for heavy quarkonium

spectroscopy. Though Lattice QCD calculations in the quenched approximation suggest a linearly increasing potential in the confinement range [2–12], a specific form of interaction potential in the full range is not yet known. At short distances relativistic effects are more important as they give rise to quark-antiquark pairs from the vacuum that in turn affect the nonrelativistic Coulomb interaction in the presence of sea quarks. The mass spectra of quarkonia is not sensitive to these relativistic effects at short distances. However, the decay properties show significant difference with inclusion of relativistic corrections. So we choose to compute the charmonium mass spectra nonrelativistically in present study. The nonrelativistic Hamiltonian for the study of heavy bound state of mesons such as $c\bar{c}$, $c\bar{b}$ and $b\bar{b}$ given by

$$H = M + \frac{p^2}{2M_{cm}} + V_{\text{Cornell}}(r) + V_{SD}(r) \tag{2.1}$$

with

$$M = m_Q + m_{\bar{Q}} \quad \text{and} \quad M_{cm} = \frac{m_Q m_{\bar{Q}}}{m_Q + m_{\bar{Q}}} \tag{2.2}$$

where m_Q and $m_{\bar{Q}}$ are the masses of quark and antiquark respectively, $\vec{p}$ is the relative momentum of the each quark and $V_{\text{Cornell}}(r)$ is the quark-antiquark potential of the type coulomb plus linear confinement (Cornell potential) given by

$$V_{\text{Cornell}}(r) = -\frac{4}{3}\frac{\alpha_s}{r} + Ar. \tag{2.3}$$

Here, $1/r$ term is analogous to the Coulomb type interaction corresponding to the potential induced between quark and antiquark through one gluon exchange that dominates at small distances. The second term is the confinement part of the potential with the confinement strength A as the model parameter. The confinement term becomes dominant at the large distances. α_s is a strong running coupling constant and can be computed as

$$\alpha_s(\mu^2) = \frac{4\pi}{(11 - \frac{2}{3}n_f)\ln(\mu^2/\Lambda^2)} \tag{2.4}$$

where n_f is the number of flavors, μ is renormalization scale related to the constituent quark masses as $\mu = 2m_Q m_{\bar{Q}}/(m_Q + m_{\bar{Q}})$ and Λ is a QCD scale which is taken as 0.15 GeV by fixing $\alpha_s = 0.1185$ [1] at the Z-boson mass.

The confinement strengths with respective quark masses are fine tuned to reproduce the experimental spin averaged ground state masses of both $c\bar{c}$ and $b\bar{b}$ mesons and they are given in Table 2.1. We compute the masses of radially and orbitally excited states without any additional parameters. Similar work has been done by [49,50,104]

and they have considered different values of confinement strengths for different potential indices. The Cornell potential has been shown to be independently successful in computing the spectroscopy of ψ and Υ families. In this chapter, we compute the mass spectra of the ψ and Υ families along with B_c meson with minimum number of parameters.

Using the parameters defined in Table 2.1, we compute the spin averaged masses of quarkonia and the excited state masses are computed employing the spin dependent part of one gluon exchange potential (OGEP) $V_{SD}(r)$ perturbatively which includes spin-spin, spin-orbit and tensor terms given by [45, 83, 109, 118]

$$V_{SD}(r) = V_{SS}(r)\left[S(S+1) - \frac{3}{2}\right] + V_{LS}(r)(\vec{L}\cdot\vec{S}) + V_T(r)\left[S(S+1) - 3(S\cdot\hat{r})(S\cdot\hat{r})\right] \quad (2.5)$$

The spin-spin interaction term gives the hyper-fine splitting while spin-orbit and

Table 2.1: Parameters for quarkonium spectroscopy

m_c	m_b	A_{cc}	A_{bb}
1.317 GeV	4.584 GeV	0.18 GeV^2	0.25 GeV^2

Table 2.2: Mass spectrum of S and P-wave charmonia (in GeV)

State	Present [131]	RQM [88]	NRQM [115]	BSE [117]	SPM [126]	RPM [100]	PM [123]	NRPM [109]	NRQM [118]	PM [120]	LQCD [11]	PDG [1]
1^1S_0	2.989	2.981	2.984	2.925	2.979	2.980	2.980	2.982	3.088	2.979	2.884	2.984
1^3S_1	3.094	3.096	3.097	3.113	3.097	3.097	3.097	3.090	3.168	3.096	3.056	3.097
2^1S_0	3.602	3.635	3.637	3.684	3.623	3.597	3.633	3.630	3.669	3.600	3.535	3.639
2^3S_1	3.681	3.685	3.679	3.676	3.673	3.685	3.690	3.672	3.707	3.680	3.662	3.686
3^1S_0	4.058	3.989	4.004	–	3.991	4.014	3.992	4.043	4.067	4.011	–	–
3^3S_1	4.129	4.039	4.030	3.803	4.022	4.095	4.030	4.072	4.094	4.077	–	4.039
4^1S_0	4.448	4.401	4.264	–	4.250	4.433	4.244	4.384	4.398	4.397	–	–
4^3S_1	4.514	4.427	4.281	–	4.273	4.477	4.273	4.406	4.420	4.454	–	4.421
5^1S_0	4.799	4.811	4.459	–	4.446	–	4.440	–	–	–	–	–
5^3S_1	4.863	4.837	4.472	–	4.463	–	4.464	–	–	–	–	–
6^1S_0	5.124	5.155	–	–	4.595	–	4.601	–	–	–	–	–
6^3S_1	5.185	5.167	–	–	4.608	–	4.621	–	–	–	–	–
1^3P_0	3.428	3.413	3.415	3.323	3.433	3.416	3.392	3.424	3.448	3.488	3.412	3.415
1^3P_1	3.468	3.511	3.521	3.489	3.510	3.508	3.491	3.505	3.520	3.514	3.480	3.511
1^1P_1	3.470	3.525	3.526	3.433	3.519	3.527	3.524	3.516	3.536	3.539	3.494	3.525
1^3P_2	3.480	3.555	3.553	3.550	3.556	3.558	3.570	3.556	3.564	3.565	3.536	3.556
2^3P_0	3.897	3.870	3.848	3.833	3.842	3.844	3.845	3.852	3.870	3.947	–	3.918
2^3P_1	3.938	3.906	3.914	3.672	3.901	3.940	3.902	3.925	3.934	3.972	–	–
2^1P_1	3.943	3.926	3.916	3.747	3.908	3.960	3.922	3.934	3.950	3.996	–	–
2^3P_2	3.955	3.949	3.937	–	3.937	3.994	3.949	3.972	3.976	4.021	4.066	3.927
3^3P_0	4.296	4.301	4.146	–	4.131	–	4.192	4.202	4.214	–	–	–
3^3P_1	4.338	4.319	4.192	3.912	4.178	–	4.178	4.271	4.275	–	–	–
3^1P_1	4.344	4.337	4.193	–	4.184	–	4.137	4.279	4.291	–	–	–
3^3P_2	4.358	4.354	4.211	–	4.208	–	4.212	4.317	4.316	–	–	–
4^3P_0	4.653	4.698	–	–	–	–	–	–	–	–	–	–
4^3P_1	4.696	4.728	–	–	–	–	–	–	–	–	–	–
4^1P_1	4.704	4.744	–	–	–	–	–	–	–	–	–	–
4^3P_2	4.718	4.763	–	–	–	–	–	–	–	–	–	–
5^3P_0	4.983	–	–	–	–	–	–	–	–	–	–	–
5^3P_1	5.026	–	–	–	–	–	–	–	–	–	–	–
5^1P_1	5.034	–	–	–	–	–	–	–	–	–	–	–
5^3P_2	5.049	–	–	–	–	–	–	–	–	–	–	–

Table 2.3: Mass spectrum of D and F-wave charmonia (in GeV)

State	Present [131]	RQM [88]	NRQM [115]	BSE [117]	SPM [126]	RPM [100]	PM [123]	NRPM [109]	NRQM [118]	PM [120]
1^3D_3	3.755	3.813	3.808	3.869	3.799	3.831	3.844	3.806	3.809	3.798
1^1D_2	3.765	3.807	3.805	3.739	3.796	3.824	3.802	3.799	3.803	3.796
1^3D_2	3.772	3.795	3.807	3.550	3.798	3.824	3.788	3.800	3.804	3.794
1^3D_1	3.775	3.783	3.792	–	3.787	3.804	3.729	3.785	3.789	3.792
2^3D_3	4.176	4.220	4.112	3.806	4.103	4.202	4.132	4.167	4.167	4.425
2^1D_2	4.182	4.196	4.108	–	4.099	4.191	4.105	4.158	4.158	4.224
2^3D_2	4.188	4.190	4.109	–	4.100	4.189	4.095	4.158	4.159	4.223
2^3D_1	4.188	4.105	4.095	–	4.089	4.164	4.057	4.142	4.143	4.222
3^3D_3	4.549	4.574	4.340	–	4.331	–	4.351	–	–	–
3^1D_2	4.553	3.549	4.336	–	4.326	–	4.330	–	–	–
3^3D_2	4.557	4.544	4.337	–	4.327	–	4.322	–	–	–
3^3D_1	4.555	4.507	4.324	–	4.317	–	4.293	–	–	–
4^3D_3	4.890	4.920	–	–	–	–	4.526	–	–	–
4^1D_2	4.892	4.898	–	–	–	–	4.509	–	–	–
4^3D_2	4.896	4.896	–	–	–	–	4.504	–	–	–
4^3D_1	4.891	4.857	–	–	–	–	4.480	–	–	–
1^3F_2	3.990	4.041	–	–	–	4.068	–	4.029	–	–
1^3F_3	4.012	4.068	–	3.999	–	4.070	–	4.029	–	–
1^1F_3	4.017	4.071	–	4.037	–	4.066	–	4.026	–	–
1^3F_4	4.036	4.093	–	–	–	4.062	–	4.021	–	–
2^3F_2	4.378	4.361	–	–	–	–	–	4.351	–	–
2^3F_3	4.396	4.400	–	–	–	–	–	3.352	–	–
2^1F_3	4.400	4.406	–	–	–	–	–	4.350	–	–
2^3F_4	4.415	4.434	–	–	–	–	–	4.348	–	–
3^3F_2	4.730	–	–	–	–	–	–	–	–	–
3^3F_3	4.746	–	–	–	–	–	–	–	–	–
3^1F_3	4.749	–	–	–	–	–	–	–	–	–
3^3F_4	4.761	–	–	–	–	–	–	–	–	–

tensor terms gives the fine structure of the quarkonium states. The coefficients of spin dependent terms of the Eq. (2.5) can be written as [83],

$$V_{SS}(r) = \frac{1}{3m_Q m_{\bar{Q}}}\nabla^2 V_V(r) = \frac{16\pi\alpha_s}{9m_Q m_{\bar{Q}}}\delta^3(\vec{r}) \tag{2.6}$$

$$V_{LS}(r) = \frac{1}{2m_Q m_{\bar{Q}} r}\left(3\frac{dV_V(r)}{dr} - \frac{dV_S(r)}{dr}\right) \tag{2.7}$$

$$V_T(r) = \frac{1}{6m_Q m_{\bar{Q}}}\left(3\frac{dV_V^2(r)}{dr^2} - \frac{1}{r}\frac{dV_V(r)}{dr}\right) \tag{2.8}$$

Where $V_V(r)$ and $V_S(r)$ correspond to the vector and scalar part of the Cornell potential in Eq. (2.3) respectively. Using all the parameters defined above, the Schrödinger equation is numerically solved using *Mathematica* notebook utilizing the Runge-Kutta method [137]. It is generally believed that the charmonia need to be treated relativistically due to their lighter masses, but we note here that the computed wave functions of charmonia using relativistic as well as nonrelativistic approaches don't show significant difference [94]. The computed mass spectra of heavy quarkonia and B_c mesons are listed in Tables 2.2–2.7.

In the ERHM approach, we use the scalar plus vector potential for the quark confinement. This method was successful in predicting the low lying hadronic properties in the relativistic schemes for quark confinement [139,140] and later it was extended to

Table 2.4: Mass spectrum of S and P-wave bottomonia (in GeV)

State	Present [131]	RQM [114]	RQM [88]	NRQM [116]	BSE [117]	SPM [127]	RPM [101]	PM [123]	NRCQM [119]	PDG [1]
1^1S_0	9.428	9.402	9.398	9.390	9.414	9.389	9.393	9.392	9.455	9.398
1^3S_1	9.463	9.465	9.460	9.460	9.490	9.460	9.460	9.460	9.502	9.460
2^1S_0	9.955	9.976	9.990	9.990	9.987	9.987	9.987	9.991	9.990	9999
2^3S_1	9.979	10.003	10.023	10.015	10.089	10.016	10.023	10.024	10.015	10.023
3^1S_0	10.338	10.336	10.329	10.326	–	10.330	10.345	10.323	10.330	–
3^3S_1	10.359	10.354	10.355	10.343	10.327	10.351	10.364	10.346	10.349	10.355
4^1S_0	10.663	10.523	10.573	10.584	–	10.595	10.623	10.558	–	–
4^3S_1	10.683	10.635	10.586	10.597	–	10.611	10.643	10.575	10.607	10.579
5^1S_0	10.956	10.869	10.851	10.800	–	10.817	–	10.741	–	–
5^3S_1	10.975	10.878	10.869	10.811	–	10.831	–	10.755	10.818	10.876
6^1S_0	11.226	11.097	11.061	10.997	–	11.011	–	10.892	–	–
6^3S_1	11.243	11.102	11.088	10.988	–	11.023	–	10.904	10.995	11.019
1^3P_0	9.806	9.847	9.859	9.864	9.815	9.865	9.861	9.862	9.855	9.859
1^3P_1	9.819	9.876	9.892	9.903	9.842	9.897	9.891	9.888	9.874	9.893
1^1P_1	9.821	9.882	9.900	9.909	9.806	9.903	9.900	9.896	9.879	9.899
1^3P_2	9.825	9.897	9.912	9.921	9.906	9.918	9.912	9.908	9.886	9.912
2^3P_0	10.205	10.226	10.233	10.220	10.254	10.226	10.230	10.241	10.221	10.232
2^3P_1	10.217	10.246	10.255	10.249	10.120	10.251	10.255	10.256	10.236	10.255
2^1P_1	10.220	10.250	10.260	10.254	10.154	10.256	10.262	10.261	10.240	10.260
2^3P_2	10.224	10.261	10.268	10.264	–	10.269	10.271	10.268	10.246	10.269
3^3P_0	10.540	10.552	10.521	10.490	–	10.502	–	10.511	10.500	–
3^3P_1	10.553	10.538	10.541	10.515	10.303	10.524	–	10.507	10.513	–
3^1P_1	10.556	10.541	10.544	10.519	–	10.529	–	10.497	10.516	–
3^3P_2	10.560	10.550	10.550	10.528	–	10.540	–	10.516	10.521	–
4^3P_0	10.840	10.775	10.781	–	–	10.732	–	–	–	–
4^3P_1	10.853	10.788	10.802	–	–	10.753	–	–	–	–
4^1P_1	10.855	10.790	10.804	–	–	10.757	–	–	–	–
4^3P_2	10.860	10.798	10.812	–	–	10.767	–	–	–	–
5^3P_0	11.115	11.004	–	–	–	10.933	–	–	–	–
5^3P_1	11.127	11.014	–	–	–	10.951	–	–	–	–
5^1P_1	11.130	11.016	–	–	–	10.955	–	–	–	–
5^3P_2	11.135	11.022	–	–	–	10.965	–	–	–	–

Table 2.5: Mass spectrum of D and F-wave bottomonia (in GeV)

State	Present [131]	RQM [114]	RQM [88]	NRQM [116]	BSE [117]	SPM [127]	RPM [101]	PM [123]	NRCQM [119]	PDG [1]
1^3D_3	10.073	10.115	10.166	10.157	10.232	10.156	10.163	10.177	10.127	–
1^1D_2	10.074	10.148	10.163	10.153	10.194	10.152	10.158	10.166	10.123	–
1^3D_2	10.075	10.147	10.161	10.153	10.145	10.151	10.157	10.162	10.122	10.163
1^3D_1	10.074	10.138	10.154	10.146	–	10.145	10.149	10.147	10.117	–
2^3D_3	10.423	10.455	10.449	10.436	–	10.442	10.456	10.447	10.422	–
2^1D_2	10.424	10.450	10.445	10.432	–	10.439	10.452	10.440	10.419	–
2^3D_2	10.424	10.449	10.443	10.432	–	10.438	10.450	10.437	10.418	–
2^3D_1	10.423	10.441	10.435	10.425	–	10.432	10.443	10.428	10.414	–
3^3D_3	10.733	10.711	10.717	–	–	10.680	–	10.652	–	–
3^1D_2	10.733	10.706	10.713	–	–	10.677	–	10.646	–	–
3^3D_2	10.733	10.705	10.711	–	–	10.676	–	10.645	–	–
3^3D_1	10.731	10.698	10.704	–	–	10.670	–	10.637	–	–
4^3D_3	11.015	10.939	10.963	–	–	10.886	–	10.817	–	–
4^1D_2	11.015	10.935	10.959	–	–	10.883	–	10.813	–	–
4^3D_2	11.016	10.934	10.957	–	–	10.882	–	10.811	–	–
4^3D_1	11.013	10.928	10.949	–	–	10.877	–	10.805	–	–
1^3F_2	10.283	10.350	10.343	10.338	–	–	10.353	–	10.315	–
1^3F_3	10.287	10.355	10.346	10.340	10.302	–	10.356	–	10.321	–
1^1F_3	10.288	10.355	10.347	10.339	10.319	–	10.356	–	10.322	–
1^3F_4	10.291	10.358	10.349	10.340	–	–	10.357	–	–	–
2^3F_2	10.604	10.615	10.610	–	–	–	10.610	–	–	–
2^3F_3	10.607	10.619	10.614	–	–	–	10.613	–	–	–
2^1F_3	10.607	10.619	10.647	–	–	–	10.613	–	–	–
2^3F_4	10.609	10.622	10.617	–	–	–	10.615	–	–	–
3^3F_2	10.894	10.850	–	–	–	–	–	–	–	–
3^3F_3	10.896	10.853	–	–	–	–	–	–	–	–
3^1F_3	10.897	10.853	–	–	–	–	–	–	–	–
3^3F_4	10.898	10.856	–	–	–	–	–	–	–	–

Table 2.6: Mass spectrum of S and P-wave B_c meson (in GeV)

State	Present [131]	PM [103]	RQM [88]	RQM [113]	RQM [138]	PDG [1]
1^1S_0	6.272	6.278	6.272	6.271	6.275	6.275
1^3S_1	6.321	6.331	6.333	6.338	6.314	–
2^1S_0	6.864	6.863	6.842	6.855	6.838	6.842
2^3S_1	6.900	6.873	6.882	6.887	6.850	–
3^1S_0	7.306	7.244	7.226	7.250	–	–
3^3S_1	7.338	7.249	7.258	7.272	–	–
4^1S_0	7.684	7.564	7.585	–	–	–
4^3S_1	7.714	7.568	7.609	–	–	–
5^1S_0	8.025	7.852	7.928	–	–	–
5^3S_1	8.054	7.855	7.947	–	–	–
6^1S_0	8.340	8.120	–	–	–	–
6^3S_1	8.368	8.122	–	–	–	–
1^3P_0	6.686	6.748	6.699	6.706	6.672	–
1^3P_1	6.705	6.767	6.750	6.741	6.766	–
1^1P_1	6.706	6.769	6.743	6.750	6.828	–
1^3P_2	6.712	6.775	6.761	6.768	6.776	–
2^3P_0	7.146	7.139	7.094	7.122	6.914	–
2^3P_1	7.165	7.155	7.134	7.145	7.259	–
2^1P_1	7.168	7.156	7.094	7.150	7.322	–
2^3P_2	7.173	7.162	7.157	7.164	7.232	–
3^3P_0	7.536	7.463	7.474	–	–	–
3^3P_1	7.555	7.479	7.510	–	–	–
3^1P_1	7.559	7.479	7.500	–	–	–
3^3P_2	7.565	7.485	7.524	–	–	–
4^3P_0	7.885	–	7.817	–	–	–
4^3P_1	7.905	–	7.853	–	–	–
4^1P_1	7.908	–	7.844	–	–	–
4^3P_2	7.915	–	7.867	–	–	–
5^3P_0	8.207	–	–	–	–	
5^3P_1	8.226	–	–	–	–	
5^1P_1	8.230	–	–	–	–	
5^3P_2	8.237	–	–	–	–	

Table 2.7: Mass spectrum of D and F-wave B_c meson (in GeV)

State	Present [131]	PM [103]	RQM [88]	RQM [113]	RQM [138]
1^3D_3	6.990	7.026	7.029	7.045	6.980
1^1D_2	6.994	7.035	7.026	7.041	7.009
1^3D_2	6.997	7.025	7.025	7.036	7.154
1^3D_1	6.998	7.030	7.021	7.028	7.078
2^3D_3	7.399	7.363	7.405	–	–
2^1D_2	7.401	7.370	7.400	–	–
2^3D_2	7.403	7.361	7,399	–	–
2^3D_1	7.403	7.365	7.392	–	–
3^3D_3	7.761	–	7.750	–	–
3^1D_2	7.762	–	7.743	–	–
3^3D_2	7.764	–	7.741	–	–
3^3D_1	7.762	–	7.732	–	–
4^3D_3	8.092	–	–	–	–
4^1D_2	8.093	–	–	–	–
4^3D_2	8.094	–	–	–	–
4^3D_1	8.091	–	–	–	–
1^3F_2	7.234	–	7.273	7.269	–
1^3F_3	7.242	–	7.269	7.276	–
1^1F_3	7.241	–	7.268	7.266	–
1^3F_4	7.244	–	7.277	7.271	–
2^3F_2	7.607	–	7.618	–	–
2^3F_3	7.615	–	7.616	–	–
2^1F_3	7.614	–	7.615	–	–
2^3F_4	7.617	–	7.617	–	–
3^3F_2	7.946	–	–	–	–
3^3F_3	7.954	–	–	–	–
3^1F_3	7.953	–	–	–	–
3^3F_4	7.956	–	–	–	–

accommodate multi-quark states with unequal quark masses [38, 39]. The detailed computation technique is given in the Chapter 3. The spin average masses of the charmonia and bottomonia are obtained using the model parameters $m_c = 1.428$ GeV, $m_b = 4.637$ GeV, $A = 2166$ MeV$^{3/2}$ [134].

In CPP_ν approach also the quarks and antiquarks are treated nonrelativistically. The interacting potential is given by

$$V(r) = -\frac{\alpha_c}{r} + Ar^\nu \tag{2.9}$$

with $\alpha_c = 4/3\alpha_s$, A is the confinement strength and ν is the general power ranges from 0.5 to 2 and $\nu = 1$ corresponds to the Cornell potential. The Schrödinger equation for the potential Eq. (2.9) is solved using the hydrogenic trial wave function given by,

$$R_{nl}(r) = \sqrt{\frac{\mu^3(n-l-1)!}{2n(n+l)!}}(\mu r)^l e^{-\mu r/2} L^{2l+1}_{n-l-1}(\mu r) \tag{2.10}$$

Here, μ is the variational parameter and $L^{2l+1}_{n-l-1}(\mu r)$ is the associated Laguerre polynomial. For the given ν, the variational parameter is determined using the virial theorem

$$\langle KE \rangle = \frac{1}{2}\left\langle r\frac{dV}{dr}\right\rangle \tag{2.11}$$

The potential parameters are $m_c = 1.31$ GeV, $m_b = 4.66$ GeV, $\alpha_c = 0.4$ for charmonia and $\alpha_c = 0.3$ for bottomonia. In this chapter, we present our results for the $\nu = 1$ only.

It is important to note that Eq. (2.3) and Eq. (2.9) for $\nu = 1$ is same but in our paper Ref. [131], the Schrödinger equation was solved numerically while in our paper Ref. [134], the Schrödinger equation was solved using the variational trial wave function.

2.3 Decay Properties

In PDG [1], the quarkonium states are reported with masses along with their decay channels and in fact the mass spectra are determined from the decay channels only. Therefore it is important to validate any potential model with not only mass spectrum but also with the decay channels without using any additional parameter. In nonrelativistic limit, the decay channels are directly related to the corresponding

Table 2.8: Leptonic decay constant of charmonia (in MeV)

State	Present [131]	PM [104]	BSE [144]	NRQM [118]	LQCD [13]	QCDSR [13]	PDG [1]
J/ψ	325.876	338	411	393	418(8)(5)	401 ± 46	416 ± 6
$\eta_c(1S)$	350.314	363	378	402	387(7)(2)	309 ± 39	335 ± 75
$\psi(2S)$	257.340	254	155	293	–	–	304 ± 4
$\eta_c(2S)$	278.447	275	82	240	–	–	–
$\psi(3S)$	229.857	220	188	258	–	–	–
$\eta_c(3S)$	249.253	239	206	193	–	–	–
$\psi(4S)$	212.959	200	262	–	–	–	–
$\eta_c(4S)$	231.211	217	87	–	–	–	–
$\psi(5S)$	200.848	186	–	–	–	–	–
$\eta_c(5S)$	218.241	202	–	–	–	–	
$\psi(6S)$	191.459	175	–	–	–	–	–
$\eta_c(6S)$	208.163	197	–	–	–	–	–

wave function. In this section, we test our potential parameters and wave function to compute the weak decays, particularly decay constants, annihilation widths and electromagnetic transitions.

2.3.1 Leptonic decay constants

The leptonic decay constants are helpful in understanding the weak decays. The matrix elements for leptonic decay constants of pseudoscalar and vector mesons are given by

$$\langle 0|\bar{Q}\gamma^{\mu}\gamma_5 Q|P_{\mu}(k)\rangle = if_P k^{\mu} \tag{2.12}$$

$$\langle 0|\bar{Q}\gamma^{\mu} Q|P_{\mu}(k)\rangle = if_V M_V \epsilon^{*\mu} \tag{2.13}$$

where k is the momentum of pseudoscalar meson, $\epsilon^{*\mu}$ is the polarization vector of meson. In the nonrelativistic limit, the decay constants of pseudoscalar and vector mesons are given by Van Royen-Weiskopf formula with QCD correction factor [141–143]

$$f^2_{P/V} = \frac{3|R_{nsP/V}(0)|^2}{\pi M_{nsP/V}}\left[1-\frac{\alpha_s}{\pi}\left(\delta^{P/V}-\frac{m_Q-m_{\bar{Q}}}{m_Q+m_{\bar{Q}}}\ln\frac{m_Q}{m_{\bar{Q}}}\right)\right]. \tag{2.14}$$

With $\delta^P = 2$ and $\delta^V = 8/3$. Using the above relation, we compute the leptonic decay constants and the results are listed in Tables 2.8 – 2.11 in comparison with other models including LQCD.

Table 2.9: Leptonic decay constant of bottomonia (in MeV)

State	Present [131]	PM [104]	BSE [144]	NRQM [118]	BSE [145]	LQCD [14]	PDG [1]
$\Upsilon(1S)$	647.250	706	707	665	498±(20)	649(31)	715 ± 5
$\eta_b(1S)$	646.025	744	756	599	–	–	–
$\Upsilon(2S)$	519.436	547	393	475	366±(27)	481(39)	498 ± 8
$\eta_b(2S)$	518.803	577	285	411	–	–	–
$\Upsilon(3S)$	475.440	484	9	418	304±(27)	–	430 ± 4
$\eta_b(3S)$	474.954	511	333	354	–	–	–
$\Upsilon(4S)$	450.066	446	20	388	259±(22)	–	336 ± 18
$\eta_b(4S)$	449.654	471	40	–	–	–	–
$\Upsilon(5S)$	432.437	419	–	367	228±(16)	–	–
$\eta_b(5S)$	432.072	443	–	–	–	–	–
$\Upsilon(6S)$	418.977	399	–	351	–	–	–
$\eta_b(6S)$	418.645	422	–	–	–	–	–

Table 2.10: Pseudoscalar decay constant of B_c meson (in MeV)

State	f_P Present [131]	PM [104]	RQM [91]	QCDSR [45]	PM [71]	RQM [138]
$1S$	432.955	465	503	460±(60)	500	554.125
$2S$	355.504	361	–	–	–	
$3S$	325.659	319	–	–	–	
$4S$	307.492	293	–	–	–	
$5S$	294.434	275	–	–	–	
$6S$	284.237	261	–	–	–	

Table 2.11: Vector decay constant of B_c meson (in MeV)

State	f_V Present [131]	PM [104]	RQM [91]	QCDSR [45]	PM [71]
$1S$	434.642	435	433	460±(60)	500
$2S$	356.435	337	–	–	–
$3S$	326.374	297	–	–	–
$4S$	308.094	273	–	–	–
$5S$	294.962	256	–	–	–
$6S$	284.709	243	–	–	–

Table 2.12: Digamma decay width of S and P-wave charmonia (in keV)

State	Present [131]	ERHM [134]	CPP_ν [134]	SPM [126]	RQM [93]	NRQM [118]	BSE [158]	PDG [1]
1^1S_0	7.231	6.21	12.99	8.5	5.5	7.18	7.14±0.95	5.1±0.4
2^1S_0	5.507	4.21	5.63	2.4	1.8	1.71	4.44±0.48	2.15±1.58
3^1S_0	4.971	2.17	3.84	0.88	–	1.21	–	–
4^1S_0	4.688	1.01	3.01	–	–	–	–	–
5^1S_0	4.507	–	–	–	–	–	–	–
6^1S_0	4.377	–	–	–	–	–	–	–
1^3P_0	8.982	71.04	27.91	2.5	2.9	3.28	–	2.34±0.19
1^3P_2	1.069	75.06	5.76	0.31	0.50	–	–	0.53±0.4
2^3P_0	9.111	5.87	146.57	1.7	1.9	–	–	–
2^3P_2	1.084	5.91	30.49	0.23	0.52	–	–	–
3^3P_0	9.104	–	–	1.2	–	–	–	–
3^3P_2	1.0846	–	–	0.17	–	–	–	–
4^3P_0	9.076	–	–	–	–	–	–	–
4^3P_2	1.080	–	–	–	–	–	–	–
5^3P_0	9.047	–	–	–	–	–	–	–
5^3P_2	1.077	–	–	–	–	–	–	–

2.3.2 Annihilation widths

In this subsection we compute $\gamma\gamma$, $\gamma\gamma\gamma$, gg, ggg, γgg and $\ell^+\ell^-$ annihilation decay widths of heavy quarkonia.

Photon annihilation widths

The measurement of digamma decay widths provides the information regarding the internal structure of meson. The decays $\eta_c \to \gamma\gamma$, $\chi_{c0,2} \to \gamma\gamma$ were reported by CLEO-c [146], *BABAR* [147] and then BESIII [148] collaboration have reported high accuracy data. LQCD is found to underestimate the decay widths of $\eta_c \to \gamma\gamma$ and $\chi_{c0} \to \gamma\gamma$ when compared to experimental data [149, 150]. Other approaches to attempt computation of annihilation rates of heavy quarkonia include NRQCD [31, 151–154], relativistic quark model [92, 93], effective Lagrangian [155, 156] and next-to-next-to leading order QCD correction to $\chi_{c0,2} \to \gamma\gamma$ in the framework of nonrelativistic QCD factorization [157].

The meson decaying into two photons suggests that the spin can never be one [160, 161]. Corresponding digamma decay width of a pseudoscalar meson in nonrel-

Table 2.13: Digamma decay width of S and P-wave bottomonia (in keV)

State	Present [131]	ERHM [134]	CPP_ν [134]	SPM [127]	RQM [112]	RQM [93]	NRQM [118]	BSE [158]
1^1S_0	0.387	0.35	0.37	0.527	0.214	0.35	0.23	0.384 ± 0.047
2^1S_0	0.263	0.20	0.10	0.263	0.121	0.15	0.07	0.191 ± 0.025
3^1S_0	0.229	0.09	0.06	0.172	0.906	0.10	0.04	–
4^1S_0	0.212	0.07	0.054	0.105	0.755	–	–	–
5^1S_0	0.201	–	–	0.121	–	–	–	–
6^1S_0	0.193	–	–	0.050	–	–	–	–
1^3P_0	0.0196	1.39	0.08	0.050	0.0208	0.038	–	–
1^3P_2	0.0052	1.40	0.018	0.0066	0.0051	0.008	–	–
2^3P_0	0.0195	0.10	0.43	0.037	0.0227	0.029	–	–
2^3P_2	0.0052	0.10	0.09	0.0067	0.0062	0.006	–	–
3^3P_0	0.0194	–	–	0.037	–	–	–	–
3^3P_2	0.0051	–	–	0.0064	–	–	–	–
4^3P_0	0.0192	–	–	–	–	–	–	–
4^3P_2	0.0051	–	–	–	–	–	–	–
5^3P_0	0.0191	–	–	–	–	–	–	–
5^3P_2	0.0050	–	–	–	–	–	–	–

Table 2.14: 3γ decay widths of charmonia (in eV) and bottomonia (in 10^{-6} keV)

State	Present	PM [159]	PDG [1]	State	Present	NRCQM [119]
J/ψ	1.36	3.95	1.08 ± 0.032	$\Upsilon(1S)$	7.05	3.44
$\psi(2S)$	1.01	1.64	–	$\Upsilon(2S)$	4.79	2.00
$\psi(3S)$	0.91	1.39	–	$\Upsilon(3S)$	4.16	1.55
$\psi(4S)$	0.85	1.30	–	$\Upsilon(4S)$	3.85	1.29
$\psi(5S)$	0.81	1.25	–	$\Upsilon(5S)$	3.64	–
$\psi(6S)$	0.79	1.22	–	$\Upsilon(6S)$	3.51	–

ativistic limit is given by Van Royen-Weiskopf formula [141, 162],

$$\begin{aligned}
\Gamma_{n^1S_0\to\gamma\gamma} &= \frac{3\alpha_e^2 e_Q^4 |R_{nsP}(0)|^2}{m_Q^2}\left[1+\frac{\alpha_s}{\pi}\left(\frac{\pi^2-20}{3}\right)\right] \\
\Gamma_{n^3P_0\to\gamma\gamma} &= \frac{27\alpha_e^2 e_Q^4 |R'_{nP}(0)|^2}{m_Q^4}\left[1+\frac{\alpha_s}{\pi}\left(\frac{3\pi^2-28}{9}\right)\right] \\
\Gamma_{n^3P_2\to\gamma\gamma} &= \frac{36\alpha_e^2 e_Q^4 |R'_{nP}(0)|^2}{5m_Q^4}\left[1-\frac{16}{3}\frac{\alpha_s}{\pi}\right]
\end{aligned} \tag{2.15}$$

Also the 3γ decay width of the vector quarkonia is given by [163]

$$\Gamma_{n^3S_1\to 3\gamma} = \frac{4(\pi^2-9)e_Q^6\alpha_e^3|R_{nS}(0)|^2}{3\pi m_Q^2}\left[1-\frac{12.6\alpha_s}{\pi}\right] \tag{2.16}$$

where the bracketed quantities are QCD next-to-leading order radiative corrections [162, 164].

Annihilation widths into gluon

Digluon annihilation of quarkonia is not directly observed in detectors as digluonic state decays into various hadronic states making it a bit complex to compute digluon annihilation widths from nonrelativistic approximations derived from first principles. The digluon decay width of pseudoscalar meson along with the QCD leading order radiative correction is given by [155, 162, 164, 165],

$$\begin{aligned}
\Gamma_{n^1S_0\to gg} &= \frac{2\alpha_s^2|R_{nsP}(0)|^2}{3m_Q^2}[1+C_Q(\alpha_s/\pi)] \\
\Gamma_{n^3P_0\to gg} &= \frac{6\alpha_s^2|R'_{nP}(0)|^2}{m_Q^4}[1+C_{0Q}(\alpha_s/\pi)] \\
\Gamma_{n^3P_2\to gg} &= \frac{4\alpha_s^2|R'_{nP}(0)|^2}{5m_Q^4}[1+C_{2Q}(\alpha_s/\pi)]
\end{aligned} \tag{2.17}$$

Also the $3g$ decay width of vector quarkonia is given by

$$\Gamma_{n^3S_1\to 3g} = \frac{10(\pi^2-9)\alpha_s^3|R_{nS}(0)|^2}{81\pi m_Q^2}\left[1-\frac{3.7\alpha_s}{\pi}\right] \tag{2.18}$$

Here, the coefficients in the bracket have values of $C_Q = 4.8$, $C_{0Q} = 9.5$, $C_{2Q} = -2.2$ for the charm quark and $C_Q = 4.4$, $C_{0Q} = 10.0$, $C_{2Q} = -0.1$ for the bottom quark [162].

Also the annihilation width into γgg given by [119],

$$\Gamma_{n^3S_1\to\gamma gg} = \frac{8(\pi^2-9)e_Q^2\alpha_e\alpha_s|R_{nS(0)}|^2}{9\pi m_Q^2}\left[1-\frac{6.7\alpha_s}{\pi}\right] \tag{2.19}$$

Table 2.15: Digluon decay width of S and P-wave charmonia (in MeV)

State	Present [131]	ERHM [134]	CPP_ν [134]	PM [120]	BSE [158]	PDG [1]
1^1S_0	35.909	19.04	124.08	22.37	19.60	26.7±3.0
2^1S_0	27.345	12.91	53.77	16.74	12.1	14.7±0.7
3^1S_0	24.683	6.64	36.64	14.30	–	–
4^1S_0	23.281	3.1	28.74	–	–	–
5^1S_0	22.379	–	–	–	–	–
6^1S_0	23.736	–	–	–	–	–
1^3P_0	37.919	0.19	0.195	9.45	–	10.4±0.7
1^3P_2	3.974	0.2	6.93	2.81	–	2.03±0.12
2^3P_0	38.462	5.31	1.02	10.09	–	–
2^3P_2	4.034	5.43	36.69	7.34	–	–
3^3P_0	38.433	–	–	–	–	–
3^3P_2	4.028	–	–	–	–	–
4^3P_0	38.315	–	–	–	–	–
4^3P_2	4.016	–	–	–	–	–
5^3P_0	39.191	–	–	–	–	–
5^3P_2	4.003	–	–	–	–	–

Table 2.16: Digluon decay width of S and P-wave bottomonia (in MeV)

State	Present [131]	ERHM [134]	CPP_ν [134]	PM [50]	BSE [158]	RPM [166]
1^1S_0	5.448	9.95	23.72	17.945	6.98	12.46
2^1S_0	3.710	5.64	6.61	–	3.47	–
3^1S_0	3.229	2.61	3.86	–	–	–
4^1S_0	2.985	2.07	3.45	–	–	–
5^1S_0	2.832	–	–	–	–	–
6^1S_0	2.274	–	–	–	–	–
1^3P_0	0.276	38.17	4.90	5.250	–	2.15
1^3P_2	0.073	38.57	0.66	0.822	–	0.22
2^3P_0	0.275	1.92	25.04	–	–	–
2^3P_2	0.073	1.92	3.39	–	–	–
3^3P_0	0.273	–	–	–	–	–
3^3P_2	0.072	–	–	–	–	–
4^3P_0	0.271	–	–	–	–	–
4^3P_2	0.072	–	–	–	–	–
5^3P_0	0.269	–	–	–	–	–
5^3P_2	0.071	–	–	–	–	–

Table 2.17: $3g$ decay widths of charmonia (in keV) and bottomonia (in keV)

State	Present	PM [159]	PDG [1]	State	Present	NRCQM [119]	PDG [1]
J/ψ	264.25	269.06	59.55	$\Upsilon(1S)$	39.15	41.63	–
$\psi(2S)$	196.05	112.03	31.16	$\Upsilon(2S)$	26.59	24.25	18.80
$\psi(3S)$	175.43	94.57	–	$\Upsilon(3S)$	23.13	18.76	7.25
$\psi(4S)$	164.66	88.44	–	$\Upsilon(4S)$	21.37	15.58	–
$\psi(5S)$	157.77	85.30	–	$\Upsilon(5S)$	20.27	–	–
$\psi(6S)$	152.86	83.19	–	$\Upsilon(6S)$	19.49	–	–

Table 2.18: γgg decay widths of charmonia (in keV) and bottomonia (in keV)

State	Present	PM [159]	PDG [1]	State	Present	NRCQM [119]	PDG [1]
J/ψ	7.51	8.90	8.17	$\Upsilon(1S)$	0.85	0.79	–
$\psi(2S)$	5.57	3.75	3.03	$\Upsilon(2S)$	0.58	0.46	0.60
$\psi(3S)$	4.99	3.16	–	$\Upsilon(3S)$	0.50	0.36	1.97
$\psi(4S)$	4.68	2.96	–	$\Upsilon(4S)$	0.46	0.30	–
$\psi(5S)$	4.48	2.85	–	$\Upsilon(5S)$	0.44	–	–
$\psi(6S)$	4.35	2.78	–	$\Upsilon(6S)$	0.42	–	–

Annihilation widths into electron

The vector mesons have quantum numbers 1^{--} and can annihilate into dilepton. The dileptonic decay of vector meson along with one loop QCD radiative correction is given by [141, 162]

$$\Gamma_{n^3S_1\to\ell^+\ell^-} = \frac{4\alpha_e^2 e_Q^2 |R_{nsV}(0)|^2}{M_{nsV}^2}\left[1-\frac{16\alpha_s}{3\pi}\right] \tag{2.20}$$

Here, α_e is the electromagnetic coupling constant, α_s is the strong running coupling constant in Eq. (2.4) and e_Q is the charge of heavy quark in terms of electron charge. In above relations, $|R_{nsP/V}(0)|$ corresponds to the wave function of S-wave at origin for pseudoscalar and vector mesons while $|R'_{nP}(0)|$ is the derivative of P-wave radial

Table 2.19: Dilepton decay width of charmonia (in keV)

State	Present [131]	RPM [123]	PM [104]	RPM [100]	RQM [92]	PDG [1]
$1S$	2.925	4.95	6.99	1.89	5.4	5.547 ± 0.14
$2S$	1.533	1.69	3.38	1.04	2.4	2.359 ± 0.04
$3S$	1.091	0.96	2.31	0.77	–	0.86 ± 0.07
$4S$	0.856	0.65	1.78	0.65	–	0.58 ± 0.07
$5S$	0.707	0.49	1.46	–	–	–
$6S$	0.602	0.39	1.24	–	–	–

Table 2.20: Dilepton decay width of bottomonia (in keV)

State	Present [131]	RPM [123]	RPM [101]	PM [104]	RQM [92]	SPM [167]	PDG [1]
$1S$	1.098	1.20	1.33	1.61	1.3	0.98	1.340 ± 0.018
$2S$	0.670	0.52	0.62	0.87	0.5	0.41	0.612 ± 0.011
$3S$	0.541	0.33	0.48	0.66	–	0.27	0.443 ± 0.008
$4S$	0.470	0.24	0.40	0.53	–	0.20	0.272 ± 0.029
$5S$	0.422	0.19	–	0.44	–	0.16	–
$6S$	0.387	0.16	–	0.39	–	0.12	–

wave function at origin. The annihilation rates of heavy quarkonia are listed in Tables 2.12 - 2.20.

2.3.3 Electromagnetic transition widths

The electromagnetic transitions can be determined broadly in terms of electric and magnetic multipole expansions and their study can help in understanding the non-perturbative regime of QCD. We consider the leading order terms i.e. electric ($E1$) and magnetic ($M1$) dipoles with selection rules $\Delta L = \pm 1$ and $\Delta S = 0$ for the $E1$ transitions while $\Delta L = 0$ and $\Delta S = \pm 1$ for $M1$ transitions. We now employ the numerical wave function for computing the electromagnetic transition widths among quarkonia and B_c meson states in order to test parameters used in present work. For $M1$ transition, we restrict our calculations for transitions among S-waves only. In the nonrelativistic limit, the radiative $E1$ and $M1$ widths are given by [16, 35, 106, 168, 169]

$$\Gamma(n^{2S+1}L_{iJ_i} \to n'^{2S+1}L_{fJ_f} + \gamma) = \frac{4\alpha_e \langle e_Q \rangle^2 \omega^3}{3}(2J_f + 1)S_{if}^{E1}|M_{if}^{E1}|^2 \quad (2.21)$$

$$\Gamma(n^3S_1 \to n'^1S_0 + \gamma) = \frac{\alpha_e \mu^2 \omega^3}{3}(2J_f + 1)|M_{if}^{M1}|^2 \quad (2.22)$$

where, mean charge content $\langle e_Q \rangle$ of the $Q\bar{Q}$ system, magnetic dipole moment μ and photon energy ω are given by

$$\langle e_Q \rangle = \left| \frac{m_{\bar{Q}} e_Q - e_{\bar{Q}} m_Q}{m_Q + m_{\bar{Q}}} \right| \quad (2.23)$$

$$\mu = \frac{e_Q}{m_Q} - \frac{e_{\bar{Q}}}{m_{\bar{Q}}} \quad (2.24)$$

$$\omega = \frac{M_i^2 - M_f^2}{2M_i} \quad (2.25)$$

Table 2.21: $E1$ transition width of charmonia (in keV)

Transition	Present [131]	ERHM [134]	$CPP\nu$ [134]	RPM [100]	RQM [91]	SPM [126]	NRQM [115]	PDG [1]
$2^3S_1 \to 1^3P_0$	21.863	9.92	38.2	45.0	51.7	74	22	29.8 ± 1.5
$2^3S_1 \to 1^3P_1$	43.292	18.6	73.6	40.9	44.9	62	42	27.9 ± 1.5
$2^3S_1 \to 1^3P_2$	62.312	11.3	37.2	26.5	30.9	43	38	26 ± 1.5
$2^1S_0 \to 1^1P_1$	36.197	–	–	8.3	8.6	146	49	–
$3^3S_1 \to 2^3P_0$	31.839	16.4	51.4	87.3	–	–	–	–
$3^3S_1 \to 2^3P_1$	64.234	43.3	65.2	65.7	–	–	–	–
$3^3S_1 \to 2^3P_2$	86.472	54.2	4	31.6	–	–	–	–
$3^3S_1 \to 1^3P_0$	46.872	129.4	583.9	1.2	–	–	–	–
$3^3S_1 \to 1^3P_1$	107.088	336.4	1531	2.5	–	–	–	–
$3^3S_1 \to 1^3P_2$	163.485	410.1	4379	3.3	–	–	–	–
$3^1S_0 \to 2^1P_1$	51.917	–	–	–	–	–	–	–
$3^1S_0 \to 1^1P_1$	178.312	–	–	–	–	–	–	–
$1^3P_0 \to 1^3S_1$	112.030	325.9	209	142.2	161	167	284	119.5 ± 8
$1^3P_1 \to 1^3S_1$	146.317	426.2	269	287.0	333	354	306	295 ± 13
$1^3P_2 \to 1^3S_1$	157.225	680.7	421	390.6	448	473	172	384.2 ± 16
$1^1P_1 \to 1^1S_0$	247.971	1076	1015	610.0	723	764	361	357 ± 280
$2^3P_0 \to 2^3S_1$	70.400	231.0	190	53.6	–	61	–	–
$2^3P_1 \to 2^3S_1$	102.672	258.9	316	208.3	–	103	–	–
$2^3P_2 \to 2^3S_1$	116.325	325.3	701	358.6	–	225	–	–
$2^1P_1 \to 2^1S_0$	163.646	611.7	843	–	–	309	–	–
$2^3P_0 \to 1^3S_1$	173.324	643.5	822	20.8	–	74	–	–
$2^3P_1 \to 1^3S_1$	210.958	661.3	962	28.4	–	83	–	–
$2^3P_2 \to 1^3S_1$	227.915	700.1	1279	33.2	–	101	–	–
$2^1P_1 \to 1^1S_0$	329.384	951.6	549	–	–	134	–	–
$1^3D_1 \to 1^3P_0$	161.504	–	–	–	423	486	272	172 ± 30
$1^3D_1 \to 1^3P_1$	93.775	–	–	–	142	150	138	70 ± 17
$1^3D_1 \to 1^3P_2$	5.722	–	–	–	5.8	5.8	7.1	≤ 21
$1^3D_2 \to 1^3P_1$	165.176	–	–	317.3	297	342	285	–
$1^3D_2 \to 1^3P_2$	50.317	–	–	65.7	62	70	91	–
$1^3D_3 \to 1^3P_2$	175.212	–	–	62.7	252	284	350	–
$1^1D_2 \to 1^1P_1$	205.93	–	–	–	335	575	362	–

respectively. Also the symmetric statistical factor is given by

$$S_{if}^{E1} = \max(L_i, L_f) \left\{ \begin{array}{ccc} J_i & 1 & J_f \\ L_f & S & L_i \end{array} \right\}^2 . \tag{2.26}$$

The matrix element $|M_{if}|$ for $E1$ and $M1$ transition can be written as

$$\left|M_{if}^{E1}\right| = \frac{3}{\omega} \left\langle f \left| \frac{\omega r}{2} j_0\left(\frac{\omega r}{2}\right) - j_1\left(\frac{\omega r}{2}\right) \right| i \right\rangle \tag{2.27}$$

$$\left|M_{if}^{M1}\right| = \left\langle f \left| j_0\left(\frac{\omega r}{2}\right) \right| i \right\rangle \tag{2.28}$$

The electromagnetic transition widths are listed in Tables 2.21 - 2.26 and also compared with experimental results as well as theoretical predictions.

Table 2.22: $E1$ transition width of bottomonia (in keV)

Transition	Present [131]	ERHM [134]	$CPP\nu$ [134]	RPM [100]	RQM [91]	SPM [127]	NRQM [116]	PDG [1]
$2^3S_1 \to 1^3P_0$	2.377	0.24	0.4	1.15	1.65	1.67	1.09	1.22 ± 0.11
$2^3S_1 \to 1^3P_1$	5.689	0.40	0.74	1.87	2.57	2.54	2.17	2.21 ± 0.19
$2^3S_1 \to 1^3P_2$	8.486	0.12	0.38	1.88	2.53	2.62	2.62	2.29 ± 0.20
$2^1S_0 \to 1^1P_1$	10.181	–	–	4.17	3.25	6.10	3.41	–
$3^3S_1 \to 2^3P_0$	3.330	0.35	0.32	1.67	1.65	1.83	1.21	1.20 ± 0.12
$3^3S_1 \to 2^3P_1$	7.936	0.82	0.62	2.74	2.65	2.96	2.61	2.56 ± 0.26
$3^3S_1 \to 2^3P_2$	11.447	0.80	0.30	2.80	2.89	3.23	3.16	2.66 ± 0.27
$3^3S_1 \to 1^3P_0$	0.594	3.91	15.4	0.03	0.124	0.07	0.097	0.055 ± 0.010
$3^3S_1 \to 1^3P_1$	1.518	9.50	41.4	0.09	0.307	0.17	0.0005	0.018 ± 0.010
$3^3S_1 \to 1^3P_2$	2.354	9.86	54.7	0.13	0.445	0.15	0.14	0.20 ± 0.03
$3^1S_0 \to 1^1P_1$	3.385	–	–	0.03	0.770	1.24	0.67	–
$3^1S_0 \to 2^1P_1$	13.981	–	–	–	3.07	11.0	4.25	–
$1^3P_2 \to 1^3S_1$	57.530	61.96	26.7	31.2	29.5	38.2	31.8	–
$1^3P_1 \to 1^3S_1$	54.927	39.58	21.3	27.3	37.1	33.6	31.9	–
$1^3P_0 \to 1^3S_1$	49.530	30.72	18.7	22.1	42.7	26.6	27.5	–
$1^1P_1 \to 1^1S_0$	72.094	62.70	37.7	37.9	54.4	55.8	35.8	–
$2^3P_2 \to 2^3S_1$	28.848	14.57	23.4	16.8	18.8	18.8	15.5	15.1 ± 5.6
$2^3P_1 \to 2^3S_1$	26.672	10.65	18.2	13.7	15.9	15.9	15.3	19.4 ± 5.0
$2^3P_0 \to 2^3S_1$	23.162	8.98	15.9	9.90	11.7	11.7	14.4	–
$2^1P_1 \to 2^1S_0$	35.578	15.67	25.4	–	23.6	24.7	16.2	–
$2^3P_2 \to 1^3S_1$	29.635	45.03	33.0	7.74	8.41	13.0	12.5	9.8 ± 2.3
$2^3P_1 \to 1^3S_1$	28.552	41.71	30.2	7.31	8.01	12.4	10.8	8.9 ± 2.2
$2^3P_0 \to 1^3S_1$	26.769	40.12	28.8	6.69	7.36	11.4	5.4	–
$2^1P_1 \to 1^1S_0$	34.815	49.57	1.07	–	9.9	15.9	16.1	–
$1^3D_1 \to 1^3P_0$	9.670	–	–	–	24.2	23.6	19.8	–
$1^3D_1 \to 1^3P_1$	6.313	–	–	–	12.9	12.3	13.3	–
$1^3D_1 \to 1^3P_2$	0.394	–	–	–	0.67	0.65	1.02	–
$1^3D_2 \to 1^3P_1$	11.489	–	–	19.3	24.8	23.8	21.8	–
$1^3D_2 \to 1^3P_2$	3.583	–	–	5.07	6.45	6.29	7.23	–
$1^3D_3 \to 1^3P_2$	14.013	–	–	21.7	26.7	26.4	32.1	–
$1^1D_2 \to 1^1P_1$	14.821	–	–	–	30.2	42.3	30.3	–

Table 2.23: $E1$ transition width of B_c meson (in keV)

Transition	Present [131]	RQM [91]	RQM [113]	PM [103]
$2^3S_1 \to 1^3P_0$	4.782	5.53	2.9	0.94
$2^3S_1 \to 1^3P_1$	11.156	7.65	4.7	1.45
$2^3S_1 \to 1^3P_2$	16.823	7.59	5.7	2.28
$2^1S_0 \to 1^1P_1$	18.663	4.40	6.1	3.03
$3^3S_1 \to 2^3P_0$	7.406	–	–	–
$3^3S_1 \to 2^3P_1$	17.049	–	–	–
$3^3S_1 \to 2^3P_2$	25.112	–	–	–
$3^3S_1 \to 1^3P_0$	6.910	–	–	–
$3^3S_1 \to 1^3P_1$	17.563	–	–	–
$3^3S_1 \to 1^3P_2$	27.487	–	–	–
$3^1S_0 \to 1^1P_1$	38.755	–	–	–
$3^1S_0 \to 2^1P_1$	27.988	–	–	–
$1^3P_2 \to 1^3S_1$	55.761	122	83	64.24
$1^3P_1 \to 1^3S_1$	53.294	87.1	11	51.14
$1^3P_0 \to 1^3S_1$	46.862	75.5	55	58.55
$1^1P_1 \to 1^1S_0$	71.923	18.4	80	72.28
$2^3P_2 \to 2^3S_1$	41.259	75.3	55	64.92
$2^3P_1 \to 2^3S_1$	38.533	45.3	45	50.40
$2^3P_0 \to 2^3S_1$	38.308	34.0	42	55.05
$2^1P_1 \to 2^1S_0$	52.205	13.8	52	56.28
$2^3P_2 \to 1^3S_1$	60.195	–	14	–
$2^3P_1 \to 1^3S_1$	57.839	–	5.4	–
$2^3P_0 \to 1^3S_1$	52.508	–	1.0	–
$2^1P_1 \to 1^1S_0$	74.211	–	19	–
$1^3D_1 \to 1^3P_0$	44.783	133	55	–
$1^3D_1 \to 1^3P_1$	28.731	65.3	28	–
$1^3D_1 \to 1^3P_2$	1.786	3.82	1.8	–
$1^3D_2 \to 1^3P_1$	51.272	139	64	–
$1^3D_2 \to 1^3P_2$	16.073	23.6	15	–
$1^3D_3 \to 1^3P_2$	60.336	149	78	–
$1^1D_2 \to 1^1P_1$	66.020	143	63	–

Table 2.24: $M1$ transition width of charmonia (in keV)

Transition	Present [131]	ERHM [134]	$CPP\nu$ [134]	RPM [100]	RQM [91]	NRQM [115]	PM [125]	PDG [1]
$1^3S_1 \to 1^1S_0$	2.722	0.703	9.68	2.7	1.05	2.39	3.28	1.58 ± 0.37
$2^3S_1 \to 2^1S_0$	1.172	0.151	0.55	1.2	0.99	0.19	1.45	0.21 ± 0.15
$2^3S_1 \to 1^1S_0$	7.506	20.51	58.13	0.0	0.95	7.80	–	1.24 ± 0.29
$3^3S_1 \to 3^1S_0$	9.927	20.521	58.13	–	–	0.088	–	–

Table 2.25: $M1$ transition width of bottomonia (in eV)

Transition	Present [131]	ERHM [134]	$CPP\nu$ [134]	RPM [100]	RQM [91]	NRQM [116]	PM [125]	PDG [1]
$1^3S_1 \to 1^1S_0$	37.668	2.33	9.13	4.0	5.8	10	15.36	–
$2^3S_1 \to 2^1S_0$	5.619	0.169	0.17	0.05	1.40	0.59	1.82	–
$2^3S_1 \to 1^1S_0$	77.173	1395	799	0.0	6.4	66	–	12.5 ± 4.9
$3^3S_1 \to 3^1S_0$	2.849	0.050	0.036	–	0.8	3.9	–	–
$3^3S_1 \to 2^1S_0$	36.177	–	–	–	1.5	11	–	≤ 14
$3^3S_1 \to 1^1S_0$	76.990	–	–	–	10.5	71	–	10 ± 2

Table 2.26: $M1$ transition width of B_c meson (in eV)

Transition	Present [131]	RQM [91]	RQM [113]	PM [103]
$1^3S_1 \to 1^1S_0$	53.109	33	80	2.2
$2^3S_1 \to 2^1S_0$	21.119	17	10	0.014
$2^3S_1 \to 1^1S_0$	481.572	428	600	495
$2^1S_0 \to 1^3S_1$	568.346	488	300	1092

2.3.4 Weak decays of B_c mesons

The decay modes of B_c mesons are different from charmonia and bottomonia because of the inclusion of different flavor quarks. Their decay properties are very important probes for the weak interaction as B_c meson decays only through weak decays, therefore have relatively quite long lifetime. The pseudoscalar state can not decay via strong or electromagnetic decays because of this flavor asymmetry.

In the spectator model [170], the total decay width of B_c meson can be broadly classified into three ways: (i) Decay of b quark considering c quark as a spectator, (ii) Decay of c quark considering b quark as a spectator and (iii) Annihilation channel $B_c \to \ell^+\nu_\ell$. The total width is given by

$$\Gamma(B_c \to X) = \Gamma(b \to X) + \Gamma(c \to X) + \Gamma(Anni) \tag{2.29}$$

In the calculations of total width, we have not considered the interference among them as all these decays lead to different channel. In the spectator approximation, the inclusive decay width of b and c quark is given by

$$\Gamma(b \to X) = \frac{9G_F^2|V_{cb}|^2 m_b^5}{192\pi^3} \tag{2.30}$$

$$\Gamma(c \to X) = \frac{9G_F^2|V_{cs}|^2 m_c^5}{192\pi^3} \tag{2.31}$$

$$\Gamma(Anni) = \frac{G_F^2}{8\pi}|V_{cb}|^2 f_{B_c}^2 M_{B_c} m_q^2 \left(1 - \frac{m_q^2}{M_{B_c^2}}\right)^2 C_q \tag{2.32}$$

Where $C_q = 3|V_{cs}|$ for D_s mesons and m_q is the mass of heaviest fermions. V_{cs} and V_{cb} are the CKM matrices and we have taken the value of CKM matrices from the PDG. G_f is the Fermi coupling constant. Here we have used the model quark masses, B_c meson mass and decay constants for the computation of total width. Here we compute the decay width of B_c meson using Eq. (2.29) and corresponding lifetime. The computed lifetime comes out to be 0.539×10^{-12} s which is in very good agreement with the world averaged mean life time $(0.507 \pm 0.009) \times 10^{-12}$ s [1].

2.4 Results and Discussion

Having determined the model parameters namely confinement strength and quark masses in Tab. 2.1, we present our numerical results. We first compute the mass spectra of the heavy quarkonia and B_c mesons. In almost all the papers based on potential models, the model parameters are independently fixed for experimental ground state masses of $c\bar{c}$, $b\bar{b}$ and $c\bar{b}$ mesons. But it is observed that the confinement strength of $c\bar{b}$ meson is the arithmetic mean of those for $c\bar{c}$ and $b\bar{b}$ mesons which discards the requirement of additional independent parameter for the B_c meson. Similar approach was used long back within QCD potential model [171]. We also compute various decay properties of heavy quarkonia and B_c mesons without additional parameter.

In Tables 2.2 - 2.5, we present our result for charmonium and bottomonium mass spectra. We compare our findings with PDG data [1], lattice QCD [11] data, relativistic quark model [88], nonrelativistic quark model [115,116,118], QCD relativistic functional approach [117], relativistic potential model [100], nonrelativistic potential models [109, 120, 123, 126, 127] and covariant constituent quark model [119]. Our results are in very good agreement with the PDG data [1]. For charmonia, our results show very good agreement with the LQCD data [11] with less than 2% deviation. Our results for charmonia and bottomonia also close to the relativistic quark model (RQM) [91] with less than 1% deviation. Our results are also consistent with other theoretical approaches. In Tables 2.6 and 2.7, we also predict the B_c meson mass spectra. Experimentally only pseudoscalar state for $n = 1$ and 2 is available and our results match well with very few % error. It is worth noting that the masses

of orbitally excited states (to be specific for $n = 1$) of charmonia is systematically lower than the other models and experimental data. This tendency decreases as one moves to higher excited states. But this trend is not there in B_c and bottomonia systems suggesting that the relativistic treatment may improve the results in lower energy regime of charmonia.

Using the mass spectra of heavy quarkonia and B_c meson, we plot the Regge trajectories in (J, M^2) and (n_r, M^2) planes where $n_r = n - 1$. The following relations are utilised [88]

$$J = \alpha M^2 + \alpha_0 \tag{2.33}$$

$$n_r = \beta M^2 + \beta_0 \tag{2.34}$$

where α, β are slopes and α_0, β_0 are the intercepts that can be computed using the methods given in Ref. [88]. In Figs. 2.1, 2.2 and 2.3, we plot the Regge trajectories. Regge trajectories from present approach and relativistic quark model [88] show similar trend i.e. for charmonium spectra, the computed mass squared fits very well to a linear trajectory and is found to be almost parallel and equidistant in both the planes. Also, for bottomonia and B_c mesons, we observe the nonlinearity in the parent trajectories. The nonlinearity increases as we go from $c\bar{b}$ to $b\bar{b}$ mesons indicating increasing contribution from the inter-quark interaction over confinement.

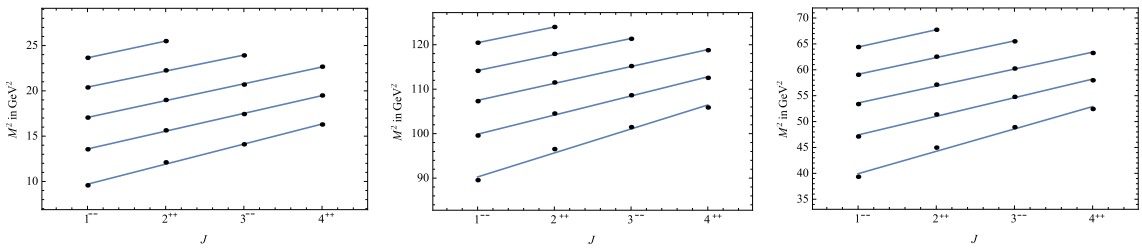

Figure 2.1: Parent and daughter Regge trajectories (J, M^2) for charmonia (left), bottomonia (middle) and B_c (right) mesons with natural parity $(P = (-1)^J)$.

Using the potential parameters and numerical wave function, we compute the various decay properties of heavy quarkonia. We first compute the leptonic decay constants of pseudoscalar and vector mesons and our numerical results are tabulated in Tables 2.8 – 2.11. For the case of charmonia, our results are higher than those using LQCD and QCDSR [13] and discrepancy removed when we include the QCD correction factors [142]. After introducing the correction factors, our results match with PDG,

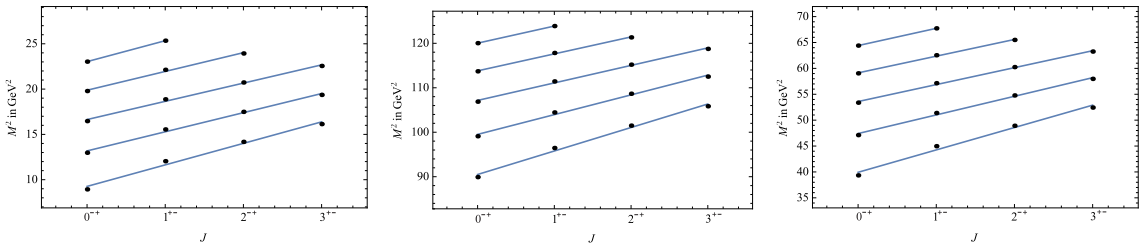

Figure 2.2: Parent and daughter Regge trajectories (J, M^2) for charmonia (left), bottomonia (middle) and B_c (right) mesons with unnatural parity $(P = (-1)^{J+1})$.

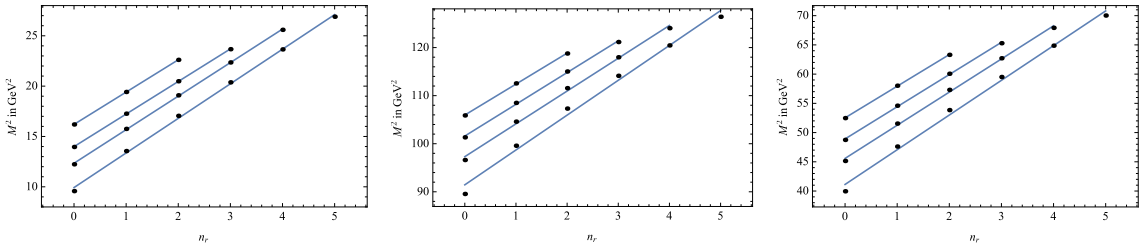

Figure 2.3: Parent and daughter Regge trajectories $(n_r \to M^2)$ for charmonia (left), bottomonia (middle) and B_c (right) mesons

LQCD and QCDSR [13] along with other theoretical models. We also compute the decay constants of bottomonia and B_c mesons. In this case, our results match with other theoretical predictions without incorporating the relativistic corrections. In the case of vector decay constants of bottomonia, our results are very close to experimental results as well as those obtained in LQCD Ref. [14]. For the decay constants of B_c mesons, we compare our results with nonrelativistic potential models [104, 138].

Then we compute the various annihilation widths of pseudoscalar and vector heavy quarkonia using the relations Eqs.(2.15)–(2.20). Where the bracketed quantities are the first order radiative corrections to the decay widths. We also compare our outcomes with the available experimental data and other theoretical results such as screened potential model (SPM) [126, 127, 167], Martin-like potential model [123], relativistic quark model (RQM) [92, 93], heavy quark spin symmetry [156], relativistic Salpeter model [158] and other theoretical models.

In Tables 2.12 and 2.13 we present our results for digamma decay widths for charmonia and bottomonia respectively. Our results for $\Gamma(\eta_c \to \gamma\gamma)$ and $\Gamma(\eta_c(2S) \to \gamma\gamma)$ are higher than the experimental data and the first order radiative correction (bracketed terms in Eq. (2.15)) was utilized to incorporate the difference and it is observed that our results along with the correction match with the data [1]. Our results for P-wave charmonia are higher than that of screened potential model [126] and rel-

ativistic quark model [93]. Our results for $\Gamma(\eta_b \to \gamma\gamma)$ match quite well with the experimental data while computed $\Gamma(\eta_b(2S) \to \gamma\gamma)$ value is overestimated when compared with the PDG data. For the excited state of S-wave bottomonia, our results fall in between those obtained in screened potential model [127] and relativistic quark model with linear confinement [114]. The scenario is similar with P-wave bottomonia and charmonia. In Tab. 2.14, we present our results for 3γ decay widths of vector quarkonia and also compared with the nonrelativistic constituent quark model [119] and potential mdoel results [159]. Our results are matching well the experimental data for the channel $J/\psi \to 3\gamma$ and other states are also inline with the others.

Digluon decay has substantial contribution to hadronic decay of quarkonia below $c\bar{c}$ and $b\bar{b}$ threshold. In Tables 2.15 and 2.16 we represent our results for digluon decay width of charmonia and bottomonia respectively. Our results for $\Gamma(\eta_c \to gg)$ match perfectly with the PDG data [1] but in the case of $\Gamma(\eta_c(2S) \to gg)$ our result is higher than the PDG data. We also compare the results obtained with that of the relativistic Salpeter method [158] and an approximate potential model [120]. It is seen from Table 2.15 that the relativistic corrections provide better results in case of P-wave charmonia where as that for bottomonia are underestimated in present calculations when compared to relativistic QCD potential model [166] and power potential model [50]. In Tab. 2.17 and 2.18 we present our results of three gluon decay and γgg decays with the comparing PDG data as well as other nonrelativistic approaches [119, 159]. It is observed that our results also in good accordance with the PDG data and theoretical models except for the channel $\psi(nS) \to 3g$.

We present the result of dilepton decay widths in the Table 2.19 and 2.20 and it is observed that our results matches with the PDG data [1] upto $n = 3$ for both charmonia and bottomonia. The contribution of the correction factor is more significant in the excited states with compared to that in the ground states of the quarkonia, indicating different dynamics in the intermediate quark-antiquark distance. Our results are also in good accordance with the other theoretical models.

Next, we present our results of $E1$ transitions in Tables 2.21 - 2.23 in comparison with theoretical attempts such as relativistic potential model [100], quark model [91], nonrelativistic screened potential model [116, 126, 127]. We also compare our results of charmonia transitions with available experimental results. We also compare our

results of ERHM and CPP_ν results [134]. Our result for $\Gamma(\psi(2S) \to \chi_{cJ}(1P) + \gamma)$ is in good agreement with the experimental result for $J = 0$ but our results for $J = 1, 2$ are higher than the PDG data. Our results also agree well for the transition $\Gamma(\chi_{c2}(1P) \to J/\psi + \gamma)$. We also satisfy the experimental constraints for the transition $\Gamma(1^3D_1 \to \chi_{cJ} + \gamma)$ for $J = 0, 1, 2$. Our results share the same range with the results computed in other theoretical models. The $E1$ transitions of bottomonia agree fairly well except for the channel $\Gamma(\Upsilon(3S) \to \chi_{bJ}(3P))$, where our results are higher than the experimental results. The comparison of our results of $E1$ transitions in B_c mesons with relativistic quark model [91, 113] and power potential model [103] are found to be in good agreement. In Tables 2.24 - 2.26, we present our results of $M1$ transitions and also compared with relativistic potential model [100], quark model [91, 114], nonrelativistic screened potential model [115, 116], power potential [103] as well as with available experimental results. Our results of $\Gamma(\mathrm{n}\psi \to \mathrm{n}'\eta_c + \gamma)$ are in very good agreement with the PDG data as well with the other theoretical predictions. Computed $M1$ transitions in B_c mesons are also within the results obtained from theoretical predictions. The computed $M1$ transition of bottomonia are found to be higher than the PDG data and also theoretical predictions. It is important to note that the experimental data of many channels are not yet available, the validity of either of the approaches can be validated only after observations in forthcoming experiments.